Nuclear Engineering and Technology 53 (2021) 2968–2976

Contents lists available at ScienceDirect

Nuclear Engineering and Technology

journal homepage: www.elsevier.com/locate/net

Original Article

3D reconstruction of two-phase random heterogeneous material from 2D sections: An approach via genetic algorithms

D. Pizzocri [a], R. Genoni [a, b], F. Antonello [a], T. Barani [a], F. Cappia [b, *]

[a] Politecnico di Milano, Department of Energy, Nuclear Engineering Division, Via La Masa 34, 20156, Milano, Italy
[b] Idaho National Laboratory, Characterization and Advanced PIE Division, 2525 Freemont Avenue, 83415 Idaho Falls, ID, United States

ARTICLE INFO

Article history:
Received 14 October 2020
Received in revised form
8 March 2021
Accepted 8 March 2021
Available online 26 March 2021

Keywords:
3D microstructure reconstruction
Genetic algorithm
Random heterogeneous material
Porosity
Nuclear fuel

ABSTRACT

This paper introduces a method to reconstruct the three-dimensional (3D) microstructure of two-phase materials, e.g., porous materials such as highly irradiated nuclear fuel, from two-dimensional (2D) sections via a multi-objective optimization genetic algorithm. The optimization is based on the comparison between the reference and reconstructed 2D sections on specific target properties, i.e., 2D pore number, and mean value and standard deviation of the pore-size distribution. This represents a multi-objective fitness function subject to weaker hypotheses compared to state-of-the-art methods based on *n*-points correlations, allowing for a broader range of application. The effectiveness of the proposed method is demonstrated on synthetic data and compared with state-of-the-art methods adopting a fitness based on 2D correlations. The method here developed can be used as a cost-effective tool to reconstruct the pore structure in highly irradiated materials using 2D experimental data.

1. Introduction

The three-dimensional microstructure of a material participates in determining its physical properties, e.g., thermal conductivity and elastic moduli, and geometrically governs transport processes, e.g., percolation [1]. Unfortunately, the 3D microstructural features of a material are very difficult to assess experimentally, with just a handful of techniques available for a limited set of materials [2]. Usually, it is way easier to experimentally extract and observe 2D sections of a material, and to perform measurements directly on the 2D sections of geometrical properties, e.g., phase fractions, porosity. This is particularly true for irradiated nuclear materials, for which handling is complicated by the extreme radioactivity, which hinders the possibility to obtain 3D experimental data further.

For this reason, several methods have been developed to infer 3D material properties from 2D sections, in general referred to as stereology [3]. Knowledge about the random medium to be reconstructed, e.g., knowing the shape of the pores, ensures that the stereological problem has a solution [4,5]. If the type of random distribution is also known, besides few unknown parameters, the problem is well posed. The latter is going to be the case analyzed in this work.

A classical methodological approach is 3D reconstruction, i.e., from a set of 2D sections, one can statistically represent 3D structures [6,7]. Among the several techniques developed and applied in the literature, gaussian filtering [8,9], maximum entropy (MaxEnt) [7], and simulated annealing (SA) [1,7,10] have proven to achieve successful 3D reconstruction results.

Any method applied to the reconstruction procedure must consider of the presence of local optima. The complex nature of the problem and the scarce knowledge of the functional space make the application of classical techniques (i.e., the Gradient Method) to solve the problem less attractive.

Besides the definition of the optimization function, there are several options for the optimization algorithm to be used to solve the reconstruction problem. However it should be reminded that the (usually) unchartered nature of the objective function—with the presence of many possible local minima, large flat plains, and points where the gradient is either undefined or discontinuous—-makes traditional analytic techniques unfit to the task [7]. Heuristic methods are more attractive since they do not depend on the characteristics of the problem, but instead leverage stochastic sampling rules on deterministic decision rules [11].

* Corresponding author.
E-mail address: fabiola.cappia@inl.gov (F. Cappia).

https://doi.org/10.1016/j.net.2021.03.012

1.1. State-of-the-art reconstruction methods

An extensive review of the available optimization algorithms applicable to 3D reconstruction is out of the scope of this work (ref. [7] provides a comprehensive review). We now briefly recall the main features of selected algorithms to contextualize the development of the herein proposed approach.

Among the state-of-the-art approaches, Gaussian filtering method is at the basis of the most commonly used 3D reconstruction techniques [1]. The method uses for reconstruction only the standard two-point probability function for reconstruction, and employs linear and nonlinear filters on Gaussian random fields (GRFs) to match the correlation function in the reconstruction process [12]. However, the conventional two-point correlation is not enough to accurately characterize the microstructure of the medium, and it is difficult to extend the method to include the other correlation functions of the biphasic isotropic media [1].

Simulated annealing (SA) [1,7,10] is a heuristic reconstruction technique based on correlations. The SA reconstruction procedure resolves to find a state of minimum *energy* among the several local minima described by the target function space by swapping the phase of the voxels of the digitized 3D random heterogeneous material (RHM)[1] [1] [7]. This swapping procedure preserves volume fractions of both phases during the reconstruction process while acting directly on the connectedness of the material phases. The resulting change in the target function, ΔT, for a certain swap is accepted with probability $p(\Delta T)$. This probability is evaluated via the Metropolis method [1]. Acting voxel-by-voxel, SA yields a very accurate description of the reconstructed 3D RHM [1,7]. Limitations to SA are the considerable computational effort required by the approach when compared to, e.g., gaussian random fields and its strong dependence on the initial conditions [7].

1.2. Genetic algorithms applied in reconstruction methods

Genetic algorithms (GA) are optimization meta-heuristic methods mimicking the biological evolution of a population in which all the individuals are candidate solutions for a given problem [13]. GA differs from GRF and SA since it (1) performs a global search and (2) can be applied as Multi-Objective Evolutionary Algorithms (MOEAs). MOEAs extend the capabilities of traditional evolutionary algorithm (e.g., SA, GRF), which are usually used to solve single objective problems, by the simultaneous optimization of several objectives, i.e., producing a set of non-dominated solutions. This approach represents a novelty in the field of application, and it is advantageous for being generally fit to the application of innovative optimization techniques. These features imply a capability of exploring the functional space. Multi-objective GA is hence generally less prone to being "trapped" into local minima compared to other methods applied to 3D reconstruction. Coherently, even if *a priori* knowledge of an approximate solution and its position in the functional space can be exploited for speed-up purpose, it is not *theoretically* strictly required [13].

The GA uses consistently more CPU time than SA and GRF, since it invests in the exploration of the solution space instead of directly converging to a minimum. GA—together with SA—has proven to be the most effective method for the 3D reconstruction of multi-phase media [1,7].

The goal of this work is to propose a 3D reconstruction procedure that is based on a GA and verify its 3D reconstruction capabilities against synthetic 3D media that are *a priori* known. We propose a 3D reconstruction approach based on an innovative definition of the target multi-objective function: to maintain the generality of the 3D reconstruction procedure, we do not use the correlation functions as the target function, since this would impose the convergence to the correlations. The correspondence of the correlations is used on the other hand for the verification of the procedure. Considering the overall characteristics, we use a GA for the solution of the optimization problem.

After a first introduction on the definitions and hypotheses necessary for the reconstruction, the frame of the GA is presented, with an description of the algorithm, the issues and limitations affecting it, and the adopted choices to overcome them.

2. Mathematical framework

In this work, we limit our analysis to the reconstruction of 3D RHM as defined by Torquato [8]. We consider a RHM composed of two domains – for simplicity, we refer to one of the two domains as *pores* [1]. The scale at which we define and describe RHMs is larger than the molecular scale and smaller than the characteristic length of the macroscopic scale. In this way, RHM is a continuum at the microscopic scale, whereas macroscopic or *effective* properties can be defined [14]. We assume that within a RHM the domains are isotropic across the volume of the RHM itself, allowing for a statistical characterization [1,2,7].

Each specific RHM can be imagined as a realization of a random process [7,14]. Thus, a two-phase RHM representing a porous medium is mathematically defined as a realization ω of a random process.

The RHM volume $V(\omega)$ is composed of volume V_1 and volume V_2 (with $V = V_1 + V_2$), corresponding to the two phases and defined by their respective volume fractions ϕ_1 (the *porosity*) and ϕ_2 (the solid matrix). Focusing on the pore phase (identified as phase 1), we define the characteristic function $I(x)$

$$I(x) = \begin{cases} 1 \text{ if } x \in V_1 \\ 0 \text{ if } x \in V_2 \end{cases} \quad (1)$$

where x is the position of a point in the volume V.

Based on the characteristic function, an RHM can be characterized by defining a set of *n-point correlations* [14,15], summarizing the statistical information about the RHM itself. In this work, we use the following three correlations [6]:

- The *one-point correlation* S_1, i.e., the probability that one random point falls within the pore phase.
- The *two-point correlation* S_2, i.e., the probability that two random points fall within the pore phase.
- The *lineal-path correlation* S_L, i.e., the probability that one random segment falls totally within the pore phase.

With these definitions and under the assumption of the RHM being stationary and ergodic[2], S_1 is independent on the position and has the same value as the pore-fraction of the medium [1], i.e.,

[1] A *random heterogeneous material* (RHM) is any material composed by two or more material phases. In this work, we assume that the RHM satisfies the isotropic hypothesis. The RHM is such that the characteristic lengths of the material phases are longer than molecular lengths and shorter than the macroscopic lengths of samples [14].

[2] The ergodic hypothesis corresponds to the assumption that the mathematical expectations can be calculated by spatial averages on the volume V, with being V sufficiently large (practically, the minimal size of the observation volume is linked to the so-called integral range [16,22]).

$$\mathbb{E}[I(x)] = S_1 = \phi_1 \tag{2}$$

with therefore $\phi_2 = 1 - \phi_1$ being the fraction of solid matrix. As for S_2, it can be shown that for an isotropic RHM it depends only on the distance between the two sampled points, $|r|$, rather than on their position [1,16], x_1 and $x_2 = x_1 + r$. Namely

$$\mathbb{E}[I(x_1)I(x_2)] = S_2(x_1, x_2) = S_2(r = x_1 - x_2) = S_2(|r|) \tag{3}$$

Moreover, it has two properties: (1) when distance between points tends to zero, it has the same value as ϕ_1, i.e., the two points are coincident, and (2) when the distance tends to infinity it has value ϕ_1^2, i.e., there is total independence of the two points. Namely

$$S_2(0) = \phi_1 \quad \text{and} \quad \lim_{r \to \infty} S_2 = \phi_1^2 \tag{4}$$

Lastly, S_L — which is the *lineal-path probability* — is introduced. Under the same hypothesis imposed in Eq. (3), this correlation depends only on the distance between two points, has value ϕ_1 for length equal to zero, and tends to zero for infinite length. Namely

$$S_L = S_L(x, x + r) = S_L(|r|) \tag{5}$$

$$S_L(0) = \phi_1 \quad \text{and} \quad \lim_{|r| \to \infty} S_L = 0 \tag{6}$$

This correlation contains information on the connectedness of the pore-phase of the component and is important to define the statistical limit threshold for percolation [1].

Under the above given ergodic assumption for an RHM and in the infinite volume limit, these correlations (Eqs. (2), (3) and (5)) for the 3D isotropic medium are identical to those of the 2D sections [1,6,14,16]. Therefore, if the hypotheses are respected, it is possible to measure these correlations on the 2D sections and directly infer the respective 3D correlations [1,6,14]. It should be remarked that identity does not hold in general and strictly depends on the fact that the 3D RHM (and the 2D section) is isotropic and ergodic [2,7,14,15]. Due to its lack of generality, the proposed 3D reconstruction technique does not enforce these identities. Nevertheless, we are going to leverage this theoretical result for the verification of the proposed 3D reconstruction technique under the above stated hypotheses [1,7].

Another fundamental characteristic of an RHM is the pore-size distribution function $P(\delta)$. It is defined as the probability that a randomly sampled point in the pore phase lies at the distance between δ and $\delta + \mathrm{d}\delta$ of the nearest point on the pore-solid interface [1].

The pore-size distribution and the other correlations herein defined are measurable in a virtual 3D RHM and in 2D sections (with in general no trivial correspondence between) by exploiting their probabilistic definition. A straightforward direct measuring technique is a Monte Carlo sampling of points within the RHM, followed by checking the conditions corresponding to each definition (e.g., is the sampled point within the porous phase?). Specific state-of-the-art techniques based on underlying Monte Carlo sampling have been developed and tailored for each correlation [1,14,15] and are adopted in this work.

3. 3D reconstruction methodology

In this section we detail the proposed 3D reconstruction technique. The main innovation brought about concerns the definition of the target multi-objective function to be minimized, whereas as optimization algorithm we adopt a multi objective GA [7]. The genetic algorithm is used since it has the best features for the resolutions of complex optimization problems defined by unknown functional space [7,11].

The fitness function F is a vector defined by the moments of the 2D pore-size distribution (i.e., average size R_{2D} and standard deviation s_{2D}) and the 2D pore number[3] N_{2D}, namely

$$F = \begin{bmatrix} \sqrt{\sum_i \left(N_{2D,\mathrm{ref}} - N_{2D,i}\right)^2} \\ \sqrt{\sum_i \left(R_{2D,\mathrm{ref}} - R_{2D,i}\right)^2} \\ \sqrt{\sum_i \left(s_{2D,\mathrm{ref}} - s_{2D,i}\right)^2} \end{bmatrix} \tag{7}$$

where the summations over i are referred to different 2D sections extracted from a 3D RHM. Remarkably, the fitness function quantities are evaluated on the 2D sections extracted from the 3D RHM. In this way, based on the properties of the 2D section, it is possible to rank the 3D microstructures as the most likely to produce sections that are statistically close to the reference section, and supposedly the 3D microstructures that are most likely to statistically match the original one. Furthermore, the optimization of a vector fitness function allows for simultaneous optimization of all its components, which is necessary to find the global optimum in a complex multi-objective problem such as the one treated in this work.

The definition of fitness provided in Eq. (7) allows overcoming hypotheses of correspondence between a 3D RHM and its 2D sections, which are commonly assumed in state-of-the-art techniques [1,2,7,8]. In general, these reconstruction techniques are based on the minimization of an objective function T describing the *distance* between the 2D section and the target 3D reconstructed RHM. A common formulation for T is [1].

$$T = \sum_{\boldsymbol{i}} \alpha_i \left(S_{2D,\mathrm{ref}}^{(i)} - S_{3D}^{(i)}\right)^2 \tag{8}$$

where α_i are weights, and i is a symbolic index defined on the above-described correlations Eqs. (2), (3) and (5)). Under the hypotheses allowing to apply Eq. (8), it is formally equivalent to use $S_{2D}^{(i)}$ instead of $S_{3D}^{(i)}$. In the following, the results obtained by using the fitness defined by Eq. (7) will be systematically compared to those achievable by the state-of-the-art fitness defined by Eq. (8).

In this work, the ranking is based on Pareto efficiency based on simultaneous confrontation between the values of all three components of the fitness function in Eq. (7).

The proposed 3D reconstruction technique initializes a first population by randomly generating a set of 3D RHMs across the space $\{N_{3D}, R_{3D}, s_{3D}\}$. Once generated, these 3D microstructures are cut at a random quote generating 2D sections that are quantitatively confronted with the reference 2D section using the fitness function (Eq. (7)). The obtained fitness value is then used to rank the cubes using Pareto efficiency based on the simultaneous minimization of all the components of fitness function (Eq. (7)).

The best individuals are selected as parents and go through the variation steps to produce the offspring. Both crossover and mutation act on the 3D parameters, generating new 3D microstructures. Once these are cut, their sections are confronted with the

[3] For a stationary point process, the number of points (i.e., centers of the objects) is a random variable, and hence it would be different for different realizations and one should consider as a parameter the point density. Nevertheless, since in the following we limit our analysis to a Poisson point process with a high number of points, the discrepancy introduced is minimal.

reference, and ranked together with their parents, again according to Pareto efficiency as mentioned above. The environmental selection saves only the fittest and kills the others for the next generation cycle. It must be stressed that, by using Pareto efficiency for ranking, the algorithm yields several individuals with the same rank, not a single one. This has the further advantage of preserving more effectively diversity in the population and better explore the search space, preventing the search to collapse in a single result.

The solutions of the reconstruction procedure evolve to minimize the difference between the reference properties of the 2D sections and the properties of the 2D sections randomly cut from reconstructed 3D media.

4. Verification and validation with synthetic data

As detailed in Section 3, the proposed technique for 3D RHM reconstruction is based on the minimization of the *distance* between a 2D reference image and the 2D sections of 3D reconstructed RHM. The assessment strategy of the proposed 3D reconstruction technique can be conceptually divided in two parts:

- The verification of the performance of the technique in localizing the minimum of the target function, i.e., the comparison of the 2D reference image with the 2D sections of the reconstructed RHM.
- The validation of the 3D reconstruction technique itself, by comparing the 3D reference RHM (from which the 2D reference image is extracted). This validation is possible because the proposed reconstruction technique performs the optimization only based on the 2D sections, without directly forcing the characteristics of the reconstructed 3D RHM.

In this section we report the results of both these assessments for a two-phase RHM made of lognormal-distributed overlapping spherical pores. The centers of the spheres are disturbed independently, i.e., according to a Poisson point process. The resulting model is therefore a Boolean model [5,16]. For all the assessment cases we consider synthetic data as reference, i.e., simulated 3D microstructures with known properties, as detailed below.

In principle, if the 2D statistical correlations of the simulated sections are close to the reference section, it is assumed that the correlations—hence the structure—of the simulated 3D media match those of the reference 3D medium. This has been extensively applied and verified [1,6–8]; however, it is important to verify if the procedure respect this theorem. The GA must be verified independently, with convergence now achieved on the pore-size distribution.

The verification is done by applying the multi objective GA to simulated ideal reference media. If convergence on the object function of the problem yields the same 2D correlations, the 3D information of the reconstructed media is also confronted with that of the reference 3D medium. If that is verified, the GA becomes applicable to the experimental results with no *a priori* knowledge of the 3D correlations. This verification must be performed on increasingly complex microstructures, ensuring that the GA can reconstruct different experimental porous media with non-ideal features.

The free parameters of the GA must also be assessed so to ensure the best efficiency of the algorithm. In this study, the free parameters of the GA are the *population size* (μ), the *selection pressure parameter* (p) for rank-based stochastic universal sampling (SUS) selection, the *crossover rate parameter*, and the *mutation rate parameter* (in this case the bitflip probability).

Population size becomes therefore crucial in defining the convergence speed [13]. An efficient population size must balance speed and accuracy of the global search. Choosing small population size eventually limits the computational cost of the GA, yet the solution will be hindered by genetic drift [17], with subsequent high risk of poor performance.

With regards to performance, selection pressure and mutation must be defined accordingly once an optimal population-size has been proposed. In presence of strong selection pressure genetic drift has little to no effect, and the population size has a weak influence, while in case of weak selection pressure the population size has an heavier role in removing genetic drift [18,19]. The effect of mutation is also important and changes in relation to the population size. When the population size is large, the mutation has ill effects on the performance of the GA, while the effect is beneficial if the population size is small [18].

Since there are few reliable theories for the determination of these parameters for better performance of the GA [13], the most feasible way in our work is direct trial and error. In this work, we present the solutions obtained for the best combinations of the hyperparameters of the GA applied to the reconstruction of different 3D RHM.

The GA ability to reproduce 3D media has been applied to a pore microstructure defined by penetrable spheres [20] whose radii follow a lognormal distribution. A lognormal distribution is described by two parameters, namely 3D average radius and 3D standard deviation radius. In this situation the 3D inputs are the 3D spherical pore number and the 3D lognormal distribution parameters. These three inputs correspond to the genes upon which the variation operators act. The reference 3D microstructure is generated with the values reported in Table 1.

The search space for reconstruction is defined accordingly to the ranges of parameters (Table 1), from which the algorithm would sample the inputs to generate the reconstructed 3D media.

The lognormal model defines a complex structure and the presence of three genes introduces further strain on the GA. However, it is a more physical distribution than the simpler ideal case of single-sized overlapping spheres, since it represents the process of statistical realization of the multiplicative product of independent random variables [21]. Convergence to the reference data is achieved on a microstructure with porosity between 0.35 and 0.40. The hyperparameters used as settings of the GA are reported in Table 2.

A different mutation rate is defined for each gene of the microstructure. This way it is expected one bit-flip per each gene on average, thus maintaining diversity while avoiding ill effects of high mutation rates on convergence [18]. This, combined with a relatively low crossover rate, allowed to achieve good convergence within few tens generations of the GA. As declared before, the set of hyperparameters herein adopted is standard for the application of GA.

The following figures show the fitness values (Figs. 1, 3 and 5) and the 2D pore-size distributions (Figs. 2, 4 and 6) for the initialization, the 10th generation, and the 20th generation (at which convergence is achieved). The axes of Figs. 1, 3 and 5 correspond to the components of the fitness function F (Eq. (7)), i.e., $\mathrm{N} = \sqrt{\sum_i (N_{2D,\mathrm{ref}} - N_{2D,i})^2}$, $\mathrm{R_m} = \sqrt{\sum_i (R_{2D,\mathrm{ref}} - R_{2D,i})^2}$, and

Table 1
Reference value of the parameters determining the 3D RHM, together with their ranges defining the search space of the 3D reconstruction algorithm.

Parameter	Reference value	Range (search space)
3D spheres number	250,000	[200,000; 300,000]
3D average sphere radius	2.15	[2.00; 2.50]
3D standard deviation of radius	2.30	[2.00; 2.50]

Table 2
Hyperparameters of the GA.

Hyperparameter	Value
Population size (μ)	100
Selection pressure (p)	1
Crossover rate	0.2
Mutation rate	1/#bit

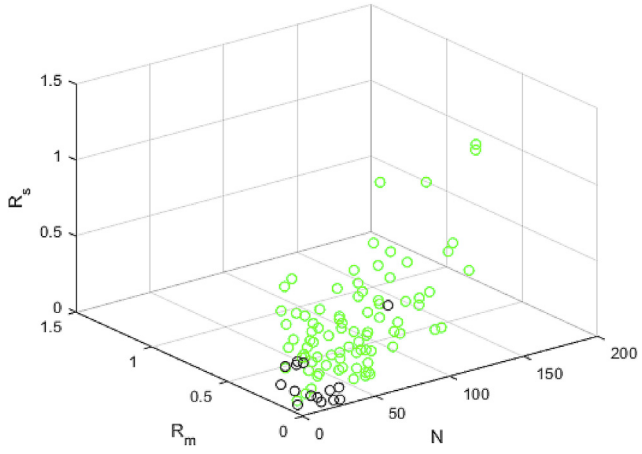

Fig. 1. Fitness values of the reconstructed media (Pareto front ones in black), initialization. (For interpretation of the references to colour in this figure legend, the reader is referred to the Web version of this article.)

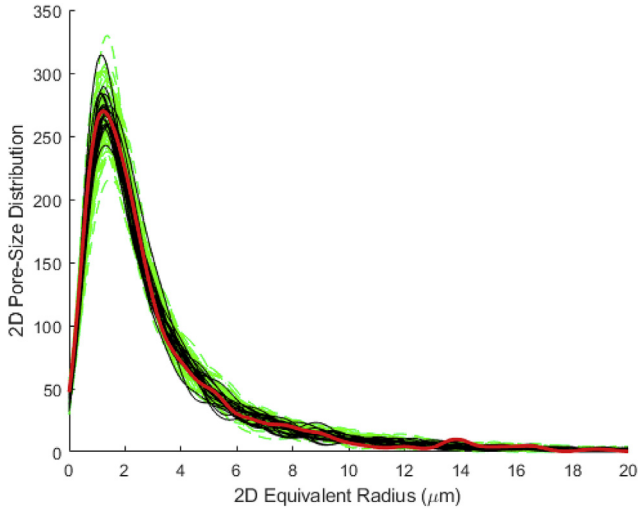

Fig. 2. Pore size distribution 2D reference (red) vs. reconstructed (green) (Pareto front in black), initialization. (For interpretation of the references to colour in this figure legend, the reader is referred to the Web version of this article.)

$R_s = \sqrt{\sum_i (s_{2D,ref} - s_{2D,i})^2}$.

As it can be observed there is a wide distribution of fitness values for the whole population in the initialization population (Fig. 1) that collapses drastically towards the origin by the 10th generation (Fig. 3). By the 20th and last generation (Fig. 5), the population is even more clustered around the origin, suggesting that good convergence of the reconstructed media to the reference has been achieved with success. This conclusion can be deduced, albeit not as clearly, by observing the 2D pore-size distributions, as progressive convergence of the pore-size distributions is achieved

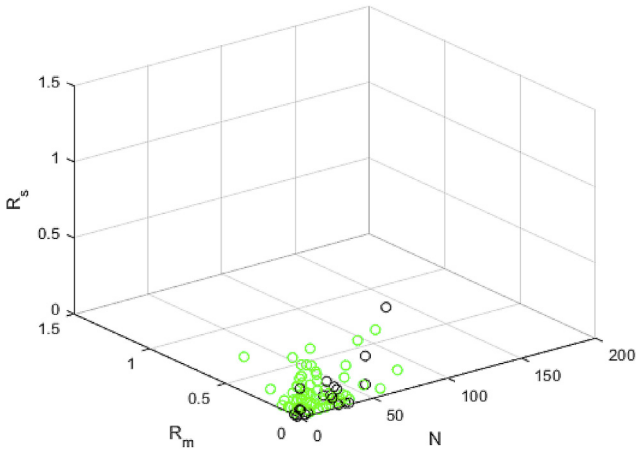

Fig. 3. Fitness values of the reconstructed media (Pareto front ones in black), generation 10. (For interpretation of the references to colour in this figure legend, the reader is referred to the Web version of this article.)

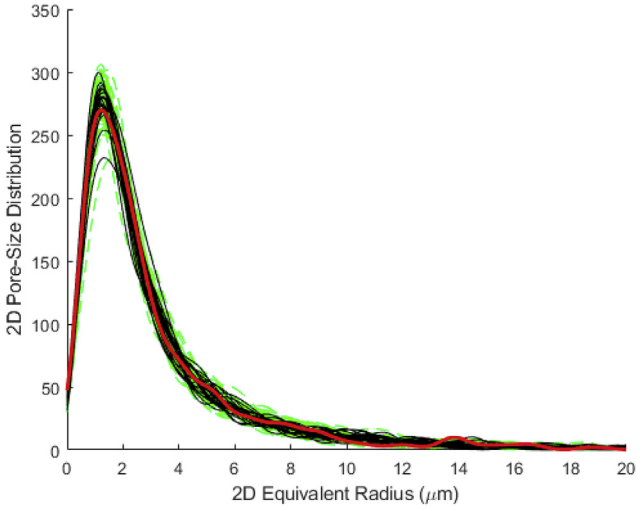

Fig. 4. Pore size distribution 2D reference (red) vs. reconstructed (green) (Pareto front in black), generation 10. (For interpretation of the references to colour in this figure legend, the reader is referred to the Web version of this article.)

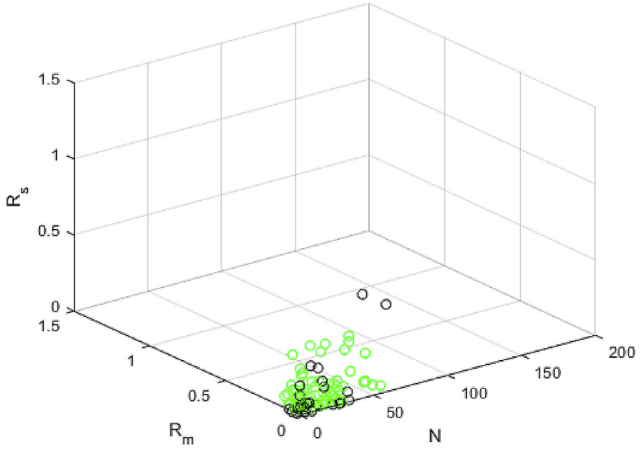

Fig. 5. Fitness values of the reconstructed media (Pareto front ones in black), generation 20. (For interpretation of the references to colour in this figure legend, the reader is referred to the Web version of this article.)

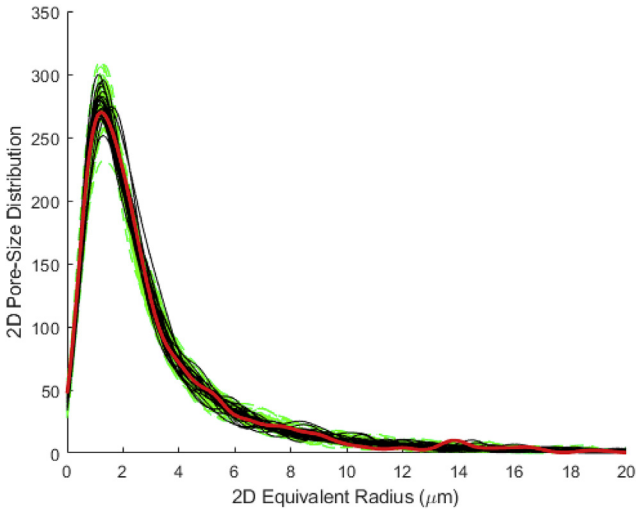

Fig. 6. Pore size distribution 2D reference (red) vs. reconstructed (green) (Pareto front in black), generation 20. (For interpretation of the references to colour in this figure legend, the reader is referred to the Web version of this article.)

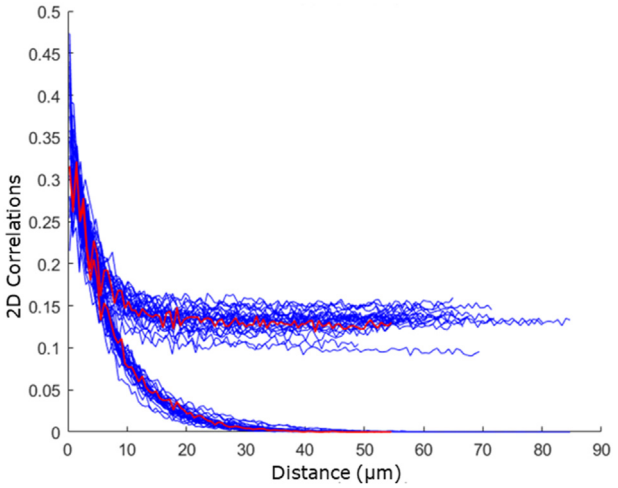

Fig. 7. 2D reference correlations (S2 curve above, SL curve below) (red) vs. 2D reconstructed correlations from the Pareto front (blue). (For interpretation of the references to colour in this figure legend, the reader is referred to the Web version of this article.)

from Figs. 2, 4 and 6.

The convergence of the fitness function also yields convergence of the 2D correlations of the reference section in the last generation, as shown in Fig. 7, where the best individuals (on the Pareto front) of the last generation are confronted with the reference. This important result verifies that the GA is able to reproduce 3D microstructures whose 2D sections are statistically close to the reference image, since the correlations are the statistical descriptors of the 2D pore phase [14].

The good results of the reconstruction procedure are noticeable from confrontation of the 2D reference section (extracted from the above described 3D RHM as a midplane horizontal cross-section, reported in Fig. 8) and a 2D section taken from one of the reconstructed media (Fig. 9), as the statistical similarity between the two can be visibly confirmed.

The GA proved effective in reproducing the 2D sections of the reference medium. The most important verification is lastly done on the confrontation of the correlations of the 3D microstructures,

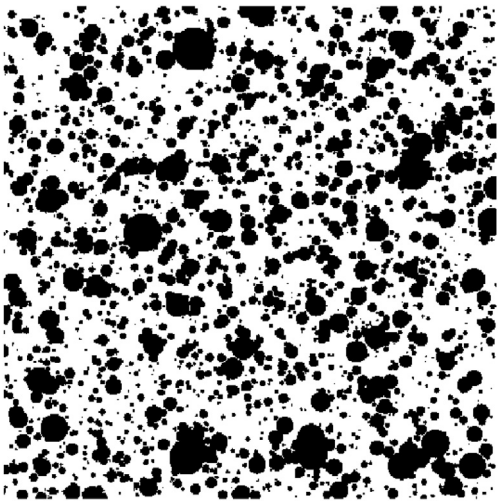

Fig. 8. Example of reference 2D section.

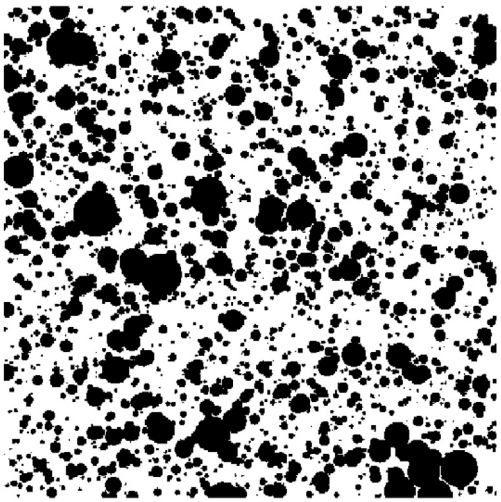

Fig. 9. Example of reconstructed 2D section.

to verify the ability of the GA reconstruct the 3D medium. The results are satisfying since convergence is achieved with minor deviations (Fig. 10), and the GA can reconstruct complex 3D microstructures constituted by overlapping spheres with lognormal-distributed radii.

For the sake of comparison, we show the results achieved by applying a state-of-the-art fitness function T, as that defined by Eq. (8). Instead of targeting the convergence on the 2D pore-size distribution, state-of-the-art approaches enforce the convergence on the 3D correlations. This convergence is hence imposed on S_1, $[\partial S_2/\partial x]_0$ (axis Lambda-S_2), and $[\partial S_L/\partial x]_0$ (axis Lambda-SL), which univocally define the correlations. The comparison between Figs. 7 and 17 shows no significant differences of reconstructing capabilities in terms of the 2D correlations. As for the convergence on the pore-size distribution, by comparing Figs. 1–6 to Figs. 11–16, it appears that the convergence is achieved more consistently with the proposed 3D reconstruction technique[4].

Validation has been performed with success on synthetic data.

[4] The relative difficulties in convergence could be explained considering that $[\partial S_2/\partial x]_0 \simeq [\partial S_L/\partial x]_0$.

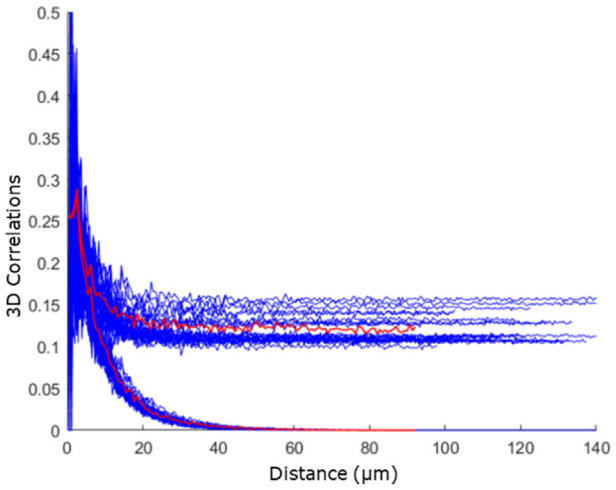

Fig. 10. 3D reference correlations (S2 curve above, SL curve below) (red) vs. 3D reconstructed correlations from the Pareto front (blue). (For interpretation of the references to colour in this figure legend, the reader is referred to the Web version of this article.)

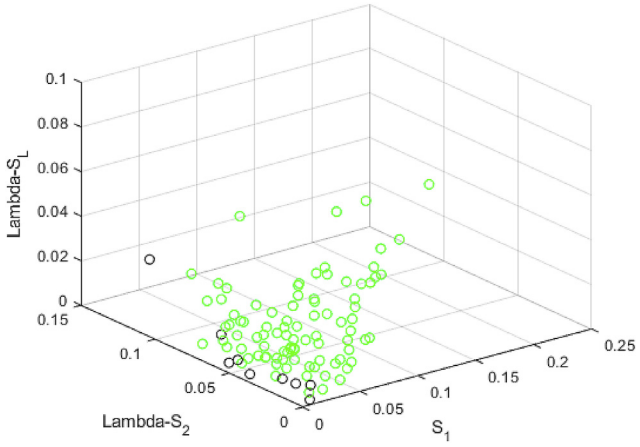

Fig. 11. Fitness values of the reconstructed media (Pareto front ones in black), initialization. (For interpretation of the references to colour in this figure legend, the reader is referred to the Web version of this article.)

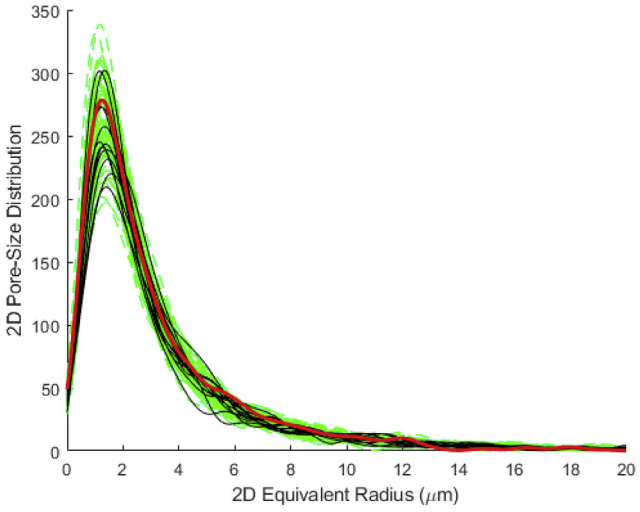

Fig. 12. Pore size distribution 2D reference (red) vs. reconstructed (green) (Pareto front in black), initialization. (For interpretation of the references to colour in this figure legend, the reader is referred to the Web version of this article.)

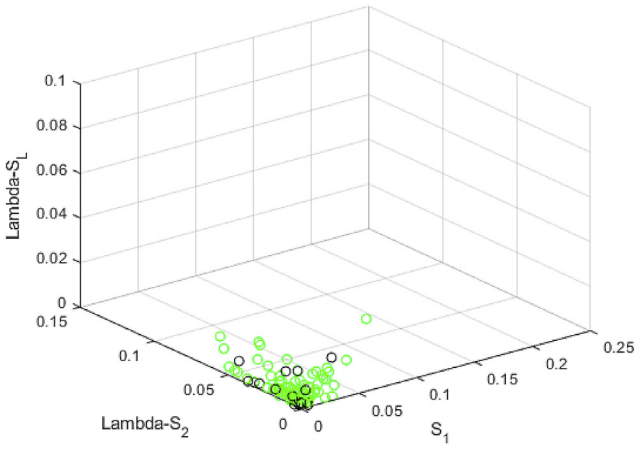

Fig. 13. Fitness values of the reconstructed media (Pareto front ones in black), generation 10. (For interpretation of the references to colour in this figure legend, the reader is referred to the Web version of this article.)

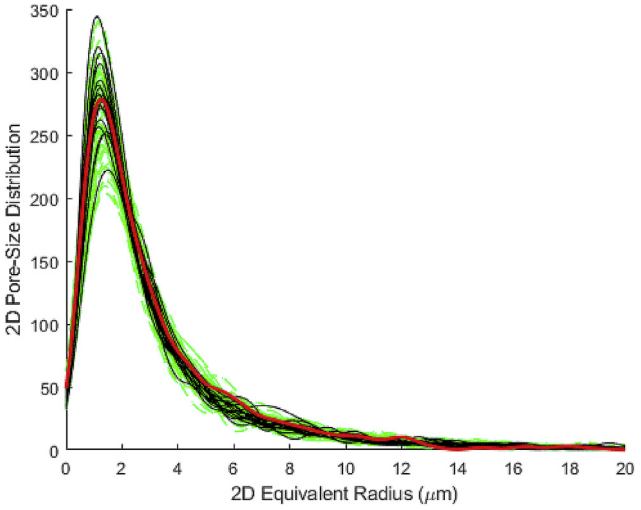

Fig. 14. Pore size distribution 2D reference (red) vs. reconstructed (green) (Pareto front in black), generation 10. (For interpretation of the references to colour in this figure legend, the reader is referred to the Web version of this article.)

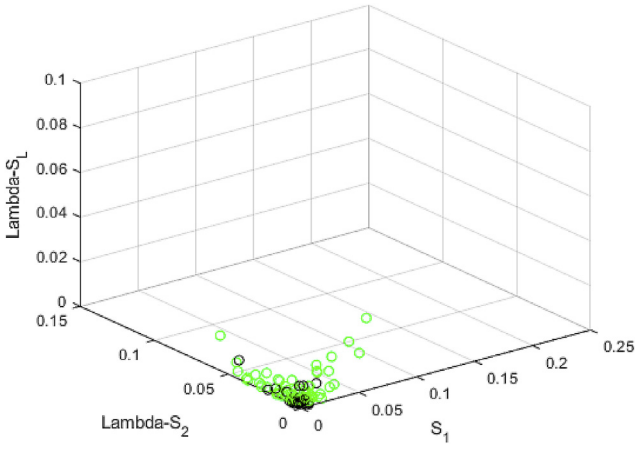

Fig. 15. Fitness values of the reconstructed media (Pareto front ones in black), generation 20. (For interpretation of the references to colour in this figure legend, the reader is referred to the Web version of this article.)

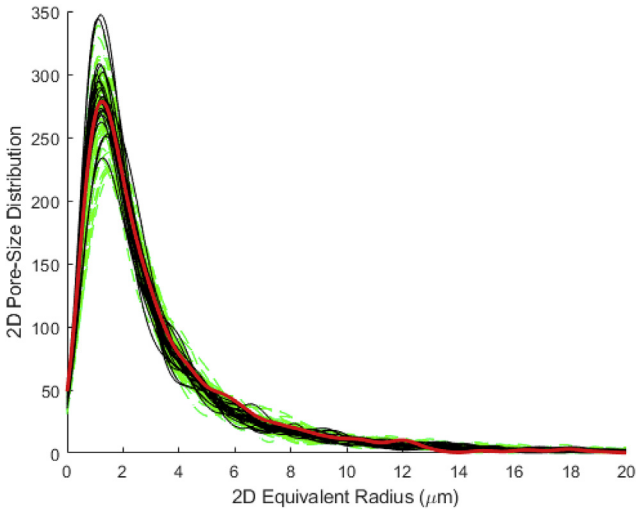

Fig. 16. Pore size distribution 2D reference (red) vs. reconstructed (green) (Pareto front in black), generation 20. (For interpretation of the references to colour in this figure legend, the reader is referred to the Web version of this article.)

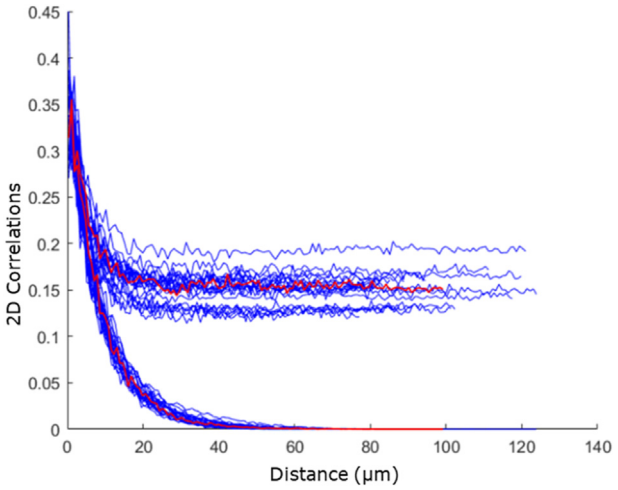

Fig. 17. 2D reference correlations (S_2 curve above, S_L curve below) (red) vs. 2D reconstructed correlations from the Pareto front (blue). (For interpretation of the references to colour in this figure legend, the reader is referred to the Web version of this article.)

The ability to reproduce the reference cube against known cubes has been proven, and the free parameters of the GA have been handled in such a way to obtain an efficient convergence to the fitness in few trials and thus in shorter times despite the high computational cost of the reconstruction procedure.

The tests on simulated data have fitted well the data, returning a good reconstruction of the pore size distribution of the 2D section of the reference media for any of the best individuals with a small variance. This also resulted in convergence to the correlations of the reference 2D section. The algorithm has therefore been assessed as the convergence on the 2D pore number, and pore average equivalent radius and standard deviation yields convergence to the correlations.

Recalling that there is correspondence between the statistical correlations of the 3D porous media and the 2D section apart from small error [14], the faithful reconstruction of the sections is expected to yield the reconstruction of the 3D media in statistical terms. This capability has been demonstrated, and the reconstruction has yielded good results.

The proposed 3D reconstruction approach is not exempt from limitations:

- It is currently limited to application to two-phase RHMs. This could be relevant in reconstructing specific nuclear materials (e.g., metallic fuel) in which one may be interested in describing more phases.
- The use of a multi-objective optimization based on 2D sections allows to relax several hypotheses which are usually enforced in classical stereological approaches but implies the need to use heuristic algorithms to solve the problem, i.e., accepting higher computational times.
- Moreover, the use of heuristic algorithms such as genetic algorithms requires considerable care in the definition of the hyperparameters, implying that the proposed approach needs to be tailored to specific applications.

5. Conclusions

We have introduced a novel approach in the reconstruction of 3D random heterogeneous material microstructure from the limited knowledge of 2D data. The proposed approach is tailored for application to porous heterogeneous materials such as highly irradiated nuclear fuels, for which direct experimental investigations are complex and expensive. The optimization method is based on a multi-objective optimization genetic algorithm. Convergence is imposed between the reference and the reconstructed 2D sections on 2D pore number, mean value and standard deviation of the pore-size distribution. This approach represents a generalization of state-of-the-art reconstruction techniques, with less constraining hypotheses and thus broader applicability. Good statistical representation of the medium is confirmed by confronting the 2D two-point correlation function and 2D lineal path function, from which 3D correlations can be inferred theoretically. The approach is verified and validated against synthetic data. Reference 3D structures with overlapping spheres whose size is logarithmically distributed, representative of highly porous materials, are reconstructed with reliable confidence. The new method has been applied to the reconstruction of the pore phase in irradiated fuel in a companion paper [23].

Declaration of competing interest

The authors declare that they have no known competing financial interests or personal relationships that could have appeared to influence the work reported in this paper.

Acknowledgments

One of the authors would like to acknowledge financial support from the U.S. Department of Energy (DOE), Office of Nuclear Energy under DOE Idaho Operations Office Contract DE-AC07-051D14517 as part of the Nuclear Science User Facilities (NSUF), Project 17–1091.

The authors greatly appreciate the reviewers who have dedicated their considerable time and expertise to this manuscript.

References

[1] C.L.Y. Yeong, S. Torquato, Reconstructing random media. II. Three-dimensional media from two-dimensional cuts, Phys. Rev. E 58 (1998) 224–233, https://doi.org/10.1103/PhysRevE.58.224.

[2] M. Yang, A. Nagarajan, B. Liang, S. Soghrati, New algorithms for virtual reconstruction of heterogeneous microstructures, Comput. Methods Appl. Mech. Eng. 338 (2018) 275–298, https://doi.org/10.1016/j.cma.2018.04.030.

[3] F. Cappia, D. Pizzocri, A. Schubert, P. Van Uffelen, G. Paperini, D. Pellottiero, R. Macián-Juan, V.V. Rondinella, Critical assessment of the pore size distribution in the rim region of high burnup UO2 fuels, J. Nucl. Mater. 480 (2016), https://doi.org/10.1016/j.jnucmat.2016.08.010.
[4] D. Nychka, G. Wahba, S. Goldfarb, T. Pugh, Cross-validated spline methods for the estimation of three-dimensional tumor size distributions from observations on two-dimensional cross sections, J. Am. Stat. Assoc. 79 (1984) 832–846.
[5] J. Serra, Image Analysis and Mathematical Morphology, 1983.
[6] C.L.Y. Yeong, S. Torquato, Reconstructing random media, Phys. Rev. E. 57 (1998) 495–506, https://doi.org/10.1103/PhysRevE.57.495.
[7] E. Patelli, G. Schuëller, On optimization techniques to reconstruct microstructures of random heterogeneous media, Comput. Mater. Sci. 45 (2009) 536–549, https://doi.org/10.1016/j.commatsci.2008.11.019.
[8] Z. Jiang, W. Chen, C. Burkhart, Efficient 3D porous microstructure reconstruction via Gaussian random field and hybrid optimization, J. Microsc. 252 (2013) 135–148, https://doi.org/10.1111/jmi.12077.
[9] Y. Jiao, F.H. Stillinger, S. Torquato, Modeling heterogeneous materials via two-point correlation functions: basic principles, Phys. Rev. E - Stat. Nonlinear Soft Matter Phys. 76 (2007) 1–15, https://doi.org/10.1103/PhysRevE.76.031110.
[10] S. Kirkpatrick, C.D. Gelatt, M.P. Vecchi, Optimization by simulated annealing, Science 220 (1983) 671–680.
[11] J. Pearl, Heuristics: Intelligent Search Strategies for Computer Problem Solving, 1984.
[12] J.A. Quiblier, A new three-dimensional modeling technique for studying porous media, J. Colloid Interface Sci. 98 (1984).
[13] A.B. Tarek, A. El-Mihoub, Adrian A. Hopgood, Lars nolle, "hybrid genetic algorithms, A Review 13 (2006) 124–137.
[14] S. Torquato, Random Heterogeneous Materials, Springer New York, New York, NY, 2002, https://doi.org/10.1007/978-1-4757-6355-3.
[15] S. Torquato, Morphology and effective properties of disordered heterogeneous media, Int. J. Solid Struct. 35 (1998) 2385–2406, https://doi.org/10.1016/S0020-7683(97)00142-X.
[16] C. Lantuéjoul, Geostatistical Simulation: Models and Algorithms, Springer, 2002.
[17] H. Furutani, S. Katayama, M. Sakamoto, T. Ito, Stochastic analysis of schema distribution in a multiplicative landscape, Artif. Life Robot. 11 (2007), 101–104. 10.1007/s10015-006-0409-5.
[18] Y.A. Zhang, M. Sakamoto, H. Furutani, Effects of population size and mutation rate on results of genetic algorithm, Proc. 4th Int. Conf. Nat. Comput. ICNC 1 (2008) 70–75, https://doi.org/10.1109/ICNC.2008.345.
[19] B.S. Weir, D.L. Hartl, Principles of population genetics, Biometrics 37 (1981) 414, 10.2307/2530432.
[20] M.D. Rintoul, S. Torquato, Precise determination of the critical threshold and exponents in a three-dimensional continuum percolation model, J. Phys. Math. Gen. 30 (1997), https://doi.org/10.1088/0305-4470/30/16/005.
[21] E. Limpert, W.A. Stahel, M. Abbt, Log-normal distributions across the sciences: keys and clues, Bioscience 51 (2006) 341, 10.1641/0006-3568(2001)051[0341:lndats]2.0.co;2.
[22] C. Lantuéjoul, Ergodicity and integral range, J. Microsc. 161 (1991) 387–403.
[23] R. Genoni, D. Pizzocri, F. Antonello, T. Barani, L. Luzzi, T.R. Pavlov, J.J. Giglio, F. Cappia, Three-dimensional reconstruction from experimental two-dimensional images: application to irradiated metallic fuel, J. Nucl. Mater. (2021), 152843, https://doi.org/10.1016/j.jnucmat.2021.152843.